ARGONNE NATIONAL LABORATORY
9700 South Cass Avenue, Argonne, Illinois 60439

ANL-ET/02-27

MODELING OF EDDY-CURRENT NDE PROBE FOR STEAM GENERATOR TUBES

by

Jimmy F. C. Chang, Sasan Bakhtiari, and David Kupperman

Energy Technology Division

June 2002

Work sponsored by
U.S. Department of Energy
Office of Nuclear Energy, Science and Technology
NEPO Program

DISCLAIMER

Contents

Figures

Tables

Nomenclature

A	Vector potential
A_{amp}	Amplitude of signal
B	Magnetic flux density
B_o	Magnetic flux density at the center of coil
E	Stored energy
H	Magnetic field intensity
J	Eddy current
N	Normal unit vector to the surface
P	Power loss
R	Mean radius of coil
r	radius
R_e	Resistance of signal
t	Time
V	Electric scalar potential
v	Volume
X	Reactance of signal
Z	Impedance of signal

Greek

ϕ	Reduced scalar potential
ψ	Total scalar potential
σ	Electrical conductivity
μ	Permeability
Ω	Integration domain
φ	Integration of magnetic flux density inside the median radius of the coil
θ	Phase angle in the impedance diagram
θ_{ref}	Reference angle (= 40^o) in normalization of impedance diagram

Modeling of Eddy-Current NDE Probe for Steam Generator Tubes*

Jimmy F. C. Chang, Sasan Bakhtiari, and David Kupperman

Energy Technology Division
Argonne National Laboratory
9700 S. Cass Avenue, IL 60439, USA

Abstract

Calculations were performed with a three-dimensional (3-D) finite-element model to describe the response of an eddy current (EC) probe to defects in steam generator (SG) tubing of a nuclear reactor. Such calculations could be very helpful in understanding and interpreting the EC probe response to complex tube/defect geometries associated with longitudinal inner/outer notches, roll transitions, sludge, and through-wall holes in SG tubes. The governing field equations are derived in terms of coupled magnetic vector and electric scalar potentials in the conducting media and total or reduced scalar potentials in the non-conducting regions. To assess the validity of the model, we compared the signal responses for two numerical approaches, stored-energy-and-power-loss approach and magnetic-flux approach for various tube/defect geometries. Simulation results are also presented on the tube/defect geometries for the pancake coil response and the transmitter/receiver (T/R) probe response. The results indicate that the eddy-current NDE modeling is capable of predicting EC probe response to flaws in steam generator tubes.

1 Introduction

The inspection of steam generator tubing is an essential element in ensuring safe and reliable operation of nuclear reactors. Detection of axial cracks in steam generator tubes is a major challenge. In recent years, the nuclear industry has made significant advances in developing probes to detect degradation in various regions of steam generator tubing. Although ultrasonic testing can be used to detect such cracks, its inspection speed is very low. Eddy-current testing requires specialized probes, and detection is often hampered by the presence of tube deformation and conducting or ferromagnetic deposits.

*Work at Argonne National Laboratory was sponsored by the U.S. Department of Energy.

Eddy-current (EC) nondestructive evaluation (NDE) techniques are currently the primary method for in-service inspection of steam generator tubing [1]. Eddy currents have proved to be useful for detecting, identifying, and characterizing flaws in metal parts [2]. Electromagnetic (EM) models have had considerable success in applying numerical methods to understanding eddy-current nondestructive testing (NDT) [3,4]. However, interpretation of EC signals is often difficult because of distortion introduced by various internal and external sources. A better understanding of the interaction of the probe with conducting media would lead to improved analysis and interpretation of signals. Exact solutions using analytical techniques [5,6], as well as two-dimensional numerical solutions [7], are limited to relatively idealized probe/defect geometries. More flexible computational techniques, such as the three-dimensional (3-D) finite-element method (FEM), are required for the analysis of more realistic probe/defect geometries. Such calculations can help in the development of appropriate characterization schemes of inspection methodology and can reduce the need for expensive experimental work. Furthermore, such models may also be used to develop a database of simulated defects with which to assess improved signal processing and data analysis techniques.

Cracks in steam generator tubes occur through a variety of mechanisms, such as stress-corrosion cracking, fatigue cracking, or inter-granular attack. They can initiate from the tube inner diameter (ID) or outer diameter (OD), and can be axial, circumferential, or branching. They occur most frequently at tube-sheet transition, support, and U-bend regions. Present industry practices/employs standard rotating pancake probes for inspection purposes, but multi-transmit/receive (T/R) array probes are now undergoing initial usage in the industry. Array probes provide higher spatial resolution and inspection speed. In this modeling study, results from both pancake coil and T/R array probes were compared.

As part of the effort to evaluate advanced EC inspection technology, array probe responses to typical calibration standard tubing defects were calculated with the 3-D FEM-based code ELEKTRA [8]. The governing EM field equations were solved by finite-element discretization in terms of magnetic vector and electric scalar potentials in conducting media and reduced or total scalar potentials in non-conducting regions. Probe impedance was determined through (1) energy and power calculations (E-P approach) for the pancake coil and (2) magnetic flux calculations (B approach) for the transmit/receive probe. The signal trajectory in the impedance plane, due to probe motion, was determined by calculating the response at discrete points along the tube axis. The 3-D modeling analysis can identify the key parameters for improved detection and sizing. This simulation could also aid in developing better data-analysis algorithms.

2 Synopsis of ELEKTRA Code

The commercial software ELEKTRA was developed by Vector Fields Inc. in England for 3-D computation of eddy currents and electromagnetic design. The ELEKTRA package includes powerful pre- and post-processing modules linked to an advanced-design analysis module that is based on research carried out at Vector Fields and Philips Research Laboratories, Eindhoven. The package has many applications and is specifically characterized by:

- 3-D time-varying EM fields,
- Time harmonic and transient fields and motion effects,
- Efficient geometry and data input facilities, and
- Comprehensive result processing and 3-D model display.

ELEKTRA uses a discrete finite-element model to solve the partial differential equations that govern the behavior of a system and includes OPERA-3D, an EM finite-element pre- and post-processor.

2.1 Model Generation

Using OPERA, we form a mesh that is automatically subdivided into elements. A two-dimensional (2-D) grid is created initially and is swept through space to create a 3-D model. The sweep operation includes facilities for rotation, projection, and translation. The mesh primitive blocks are assigned orientation and material characteristics. The resultant input is fed directly into the analysis module.

2.2 Analysis Module

ELEKTRA solves the 3-D magnetic field equations, which vary with time. The time variation can either be transient or alternating (steady state). In addition, the effects due to motion can be computed. Total and reduced magnetic scalar potentials are used for nonconducting media to reduce the solution costs and correct the cancellation errors associated with the simple reduced-potential approach. In conducting media, the program uses magnetic-vector and electric-scalar potentials, which are directly coupled with the potentials on the exterior. The use of magnetic vector and electric scalar potentials enables accurate modeling of both solutions and differing conductors in contact.

2.3 Post-processing

OPERA will display the results of the analysis in several ways, including:

- 3-D model views from any angle,
- Graphs, histograms, and contour maps of the solutions,
- Contours of components of the results on any surface,

• Calculation of fields, forces, and energy,
• Particle tracking, and
• User-defined function

3 Eddy-Current NDE Probes

3.1 Pancake Coil Probe

Current in-service inspections of steam generators involve two steps. The first is to screen the thousands of feet of tubing with a bobbin coil probe, which is very fast moving but has low resolution. Any suspicious indications are examined further by a very slow moving rotating probe that provides information on whether the flaw is ID or OD and axial or circumferential. In addition, the rotating probe provides much higher spatial resolution than the bobbin coil. Some flaw depth information can also be generated by rotating probes. Combining the two probes is time consuming and expensive, and some flaws that could be detected and characterized by a rotating probe are missed because there is no bobbin coil signal to trigger a more thorough look. Industry is developing an array probe that has significant advantages. The array probe, made up of many eddy current coils in a bracelet configuration, can be moved through the tubing at the same speed as a bobbin coil probe, while providing the detection and characterization capability of a conventional rotating probe. In one design, the array probes made up of many pancake coils will provide good coverage of the tubing and adequate spatial resolution. Sophisticated automated signal processing involving filters, deconvolution, multivariate regression algorithms, and neutral networks will minimize the difficulties in signal processing currently encountered with prototype arrays under development by industry. For this study, the probe was first evaluated with a sophisticated computer modeling program to evaluate the probe performance for the signal sensing algorithm needs, such as the number of pancake coils required by the array probe for spatial diagnostic accuracy.

3.2 Transmit/Receive Probe

A newly designed (T/R) array probe has also recently been introduced into the nuclear industry for steam generator tube inspections. This probe is made of pairs of pancake-like transmit and receive coils. The transmit coil is separated from the receive coil by a distance. Magnetic flux and eddy current originating from the transmit coil are detected in the receive coil. Qualification of this probe is ongoing. This probe is capable of detecting tube degradation at all tube locations and operating at a high inspection speed. This probe has the potential for significantly shortening inspection schedules and reducing inspection costs. Its current limitation is that the quantity of the data acquired cannot be efficiently analyzed in a manual mode. A numerical method to analyze the characteristics of inspection methodology and validate the data of the

probe will aid the development of automated data analysis techniques, which should reduce the dependency on measurement and costs associated with large teams of data analysts.

Conventional EC bobbin probes are known to be ineffectual in detecting circumferential cracks in tubing. Multipancake and/or rotating pancake probes are required to detect circumferential notches. In steam generator tubes with deformation, ferromagnetic deposits, and copper deposits, multi-channel probes with T/R coils have been demonstrated as superior to those using surface impedance coils. In addition, T/R probes have been found to be less sensitive to magnetite deposits and possess good phase discrimination to internal defects.

The successful completion of this project is dependent on whether the modeling of the probe provides the necessary information on its performance. To that end, we are developing software-based methodology to quickly, accurately, and consistently detect and characterize steam-generator tubing flaws using the signal response obtained from the model described below.

4 Modeling Methodology

The governing field equations, used in the 3-D FEM problem space, are given next. In the conducting regions, these equations are expressed in terms of the magnetic vector potential A and electric scalar potential V where μ is permeability, and σ is conductivity. In nonconducting regions, these equations are expressed in terms of either total ψ or reduced ϕ scalar potentials. Application of the Coulomb or Lorentz gauge, respectively, would allow simultaneous solution of coupled or de-coupled vector and scalar potential equations. In conducting media, where the induced eddy currents flow, the governing equations can be written as

$$\nabla \times \frac{1}{\mu} \nabla \times \vec{A} - \nabla \frac{1}{\mu} \nabla \bullet \vec{A} + \sigma \frac{\partial \vec{A}}{\partial t} + \sigma \nabla V = 0$$

$$\nabla \bullet \sigma \nabla V + \nabla \bullet \sigma \frac{\partial \vec{A}}{\partial t} = 0$$

In non-conducting regions that contain the impressed current sources, the scalar potential equations are

$$\nabla \bullet \mu \nabla \phi - \nabla \bullet \mu \left(\int_{\Omega} \frac{\vec{J} \times \vec{R}}{\left| \vec{R} \right|^3} d\Omega \right) = 0$$

$$\nabla \bullet \mu \nabla \psi = 0$$

which are then solved by finite-element discretization. The intrinsic electrical properties of each medium are incorporated through the permeability μ and the conductivity σ.

Finite-element discretization is used to solve the electromagnetic field equations in terms of magnetic vector and electric scalar potentials in conducting media and reduced or total scalar potentials in nonconducting regions. Probe impedance is determined through energy and power calculations and is interpreted through changes in the resistance and reactance of the coil. Both signal amplitude and phase from the impedance diagram are used to characterize signal response.

4.1 Pancake Coil (E-P Approach)

In all cases, stored energy and power loss were integrated in model simulations to predict the trends of impedance variation (reactance and resistance) for different setup combinations. The resistance is defined from power loss, while the reactance is defined from stored energy of the whole system. The magnitude of signal detected by the sensor is determined from the square root of resistance squared plus reactance squared. The impedance diagram serves as a tool for observing the correlation between resistance and reactance of the probe to characterize EC signals.

In the pancake coil, the quantities of interest for EC NDE, namely, the change in the coil resistance and reactance for impedance probes, can be determined through stored energy (E) and power loss (P) calculations [9]:

$$E = \frac{1}{2}\int_v \vec{B} \bullet \vec{H} dv$$

$$P = \int_v \frac{J^2}{\sigma} dv$$

where B is magnetic flux density, H is magnetic field strength, J is current density, V is volume, and σ is electrical conductivity. This calculational approach is denoted here as the E-P approach.

4.2 T/R Probe (B Approach)

The T/R probe is assumed to be composed of one transmitter and one receiver. The receiver physically exists, but it is not simulated in the model. In post-processing, the active coil (transmitter) is erased, then the integration option for fields over the area (from center to mean radius) of the receiver is used. The magnetic flux φ in the receiver coil (receiver assumed, but not simulated in the model) is approximated by the integral of the flux density along the axis of the receiver:

$$\varphi = \int_0^{(R_1+R_2)/2} 2\pi r B dr = B_o \pi \left(\frac{R_1 + R_2}{2} \right)^2$$

Flux is in phase with current, and voltage is 90 degree out of phase with flux. The reactance is at phase 0 degree, and resistance is at phase 90 degrees. In a T/R probe, the signal response is determined through the calculations of magnetic flux density (B) at phases 0 and 90 degrees. This calculational approach is denoted as the B approach.

4.3 Amplitude and Impedance Diagram

In EC NDE modeling, the signal response is composed of resistance (R_e) and reactance (X) in the complex format:

$$Z = R_e + iX$$

For the pancake coil (E-P approach), the change in the coil reactance X and coil resistance R_e for impedance probes can be determined through stored energy (E) and power loss (P) calculations:

$$X = \frac{E_{\%} - E_{0\%}}{E_{ref}}$$

$$R_e = \frac{P_{\%} - P_{0\%}}{2(2\pi f)E_{ref}}$$

Here, E_{ref} is the stored energy at the reference state, and f is the eddy-current frequency used to excite the coil. Subscript 0% indicates the reference state where there is no notch/hole is present in the steam generator tubing. Subscript % has to do with the depth of flaw indicates the state where a notch/hole exists in the steam generator tubing.

In the T/R probe (B approach), the change in the coil reactance X and coil resistance R_e for impedance probes can be determined through the calculations of magnetic flux density (B) at phases 0^o and 90^o, respectively:

$$X = \frac{B_{\%(0^o)} - B_{0\%(0^o)}}{B_{ref}}$$

$$R_e = \frac{B_{\%(90^o)} - B_{0\%(90^o)}}{B_{ref}}$$

Here, B_{ref} is the magnetic flux density at the reference state. Subscripts "0%(0^o)" and "0%(90^o)" indicate the states at phases 0 and 90 degrees where there is no notch/hole present in the steam generator tubing. Subscripts "%(0^o)" and "%(90^o)" indicate the states at phases 0 and 90 degrees

where a notch/hole exists in the steam generator tubing. Signal amplitude (A_{amp}) is used to indicate the signal magnitude detected by the probe. The amplitude is calculated as the square root of resistance squared plus reactance squared in both the pancake coil (E-P approach) and the T/R probe (B approach):

$$A_{amp} = \sqrt{(R_e^{\,2} + X^2)}$$

The impedance diagram is used for the correlation between resistance and reactance that determines the probe response to a discontinuity . The impedance diagram is also used to examine the amplitude scaling and phase alignment of the signal.

Any point on the impedance diagram is defined by

$$Z = R_e + iX = \left|A_{amp}\right| e^{i\theta} = \left|A_{amp}\right| e^{\,i\tan^{-1}\left(\frac{X}{R_e}\right)}$$

with phase angle as being:

$$\theta = \tan^{-1}\frac{X}{R_e}$$

To compare the signal change in probe for all test conditions, the normalized impedance diagram is used by introducing the reference phase angle θ_{ref} and adjusting θ_{ref} to a fixed value (e.g. $40^{o)}$:

$$Z^{norm} = Ze^{i\Delta\theta} = \left|A_{amp}\right| e^{i\theta} e^{i\Delta\theta} = \left|A_{amp}\right| e^{i(\theta+\Delta\theta)}$$

Here, θ is defined as the difference between the reference angle and the real phase angle:

$$\Delta\theta = \theta_{ref} - \theta$$

Therefore, the normalization of impedance is defined as

$$Z^{norm} = \left|A_{amp}\right| e^{i\left(\theta+\theta_{ref}-\theta\right)} = \left|A_{amp}\right| e^{i\left(\theta_{ref}\right)} = \left|A_{amp}\right| e^{i\left(40^o\right)}$$

This normalization is used in all impedance diagrams for the ease of comparison and standardization of the EC NDE model. The preprocessor stage of the software, which is based on computer-aided design, allows generation and discretization of the finite-element mesh containing the model geometry. Analysis and display of the solutions are carried out at the post-processing stage.

4.4 Boundary Conditions

Boundary conditions are used in two ways. Firstly, they can reduce the size of finite element representation for symmetrical geometries. Secondly, they can approximate the field at large distances from the problem (far-field boundaries). Problem symmetry and the symmetry of the fields are implied by the potential boundary conditions applied to the finite element model. The simplest types of boundary condition are shown in Table 1.

In Table 1, **n** is the normal unit vector to the surface being considered; **H** and **A** are magnetic field intensity and vector potential, respectively. Note that in Table 1, ϕ refers to either the reduced or total scalar potential, and V refers to the electric scalar potential. A nonzero value for V on an external surface can be used as the driving current in a problem space. Boundary conditions on the reduced scalar potential only affect the reduced field intensity. The boundary conditions shown in Table 1 should only be applied to the exterior surfaces of the finite element model.

Table 1. Boundary conditions used in modeling of steam generator tubing

	Field Symmetry	Scalar Potential	Vector Potential
Tangential Magnetic Normal Electric	$\mathbf{H} \bullet \mathbf{n} = 0$	$d\phi/dn = 0$	$\mathbf{A} \times \mathbf{n} = 0$ $V = 0$
Normal Magnetic Tangential Electric	$\mathbf{H} \times \mathbf{n} = 0$	ϕ = constant	$(\nabla \times \mathbf{A}) \times \mathbf{n} = 0$ $\mathbf{A} \bullet \mathbf{n} = 0$ $dV/dn = 0$

5 Configuration of Test Groups

5.1 Pancake Coil for Signal Response

Tube System:

Representative tube test cases simulated steady-state alternating-current (AC) solutions obtained with both pancake coil and T/R probes. The tube was modeled with inner diameter of 19.68 mm (0.775 in.), outer diameter of 22.22 mm (0.87 in.), thickness of 1.27 mm (0.05 in.), and axial length of 60 mm. A measured conductivity of 1000 Siemens/mm was used to simulate Alloy

#600 tubing material. Axial notches were simulated with various through-wall (TW) depths (100%, 80%, and 60%). The notches representing flaws had an expansion angle of 0.5° (crack width) and a length of 12.7 mm (0.5 in.).

Pancake Coil:

The pancake coil had an inner diameter of 0.5 mm (0.02 in.), outer diameter of 2.92 mm (0.115 in.), and thickness of 0.25 mm (0.0098 in.). As shown in Fig. 1, the pancake coil was circumferentially rotated in small steps (0°, 2°, 5°, 9°, 16°, and 20°) relative to the notch during tests performed at multiple frequencies (200 and 400 kHz). The sludge layer and the roll transition of the tube were simulated. In the case of the sludge layer (Fig. 2), the sludge thickness was assumed to be 6.35 mm, and its extent was determined by the subtended angle from the center of the tube (4.5°, 60°, and 180°).. For the roll transition (Fig. 3), the distance between the coil and the tube inner surface was varied between 0.875 and 2.0 mm, respectively. The test cases with the pancake coil are listed in Table 2.

5.2 T/R Probe

In the T/R probe setup for calculating the signal response, we used the same problem geometry as the one in the pancake coil setup. The T/R probe is made of two coils: transmit coil and receive coil (Fig. 4). The transmit coil has OD of 3.2 mm and ID of 1.2 mm. The receive coil has OD of 2.2 mm and ID of 1.2 mm. Both coils have thickness of 0.8 mm. The lift-off distance between coil and tube is 0.875 mm for both coils. To validate the T/R probe approach, we performed tests for the cases (1) roll transitions and (2) 80% and 40% notches from the tube outer surface at frequencies of 200 and 400 kHz, respectively.

In addition to the tests mentioned above, the T/R probe results were validated by modeling a hole at different depth levels, TW 100% and TW 80%, from the outer tube surface. The hole was varied with diameters of 1.27 mm (0.05 in.) and 0.90 mm (0.035 in.). The distance between the transmit coil and the receive coil was varied at 1.25, 1.50, and 1.75 mm. A set of tests with the hole is shown in Fig. 5. Many test cases were analyzed for different setup configurations. To analyze the sensing capability of the T/R probe, special tests were also conducted with both transmit and receive coils moving radically away from the hole. The test cases for the T/R probe are detailed in Table 3.

The results from the T/R probe (B-approach) were compared with those from the pancake coil (E-P approach). The comparison showed the consistency between these two approaches.

Table 2. Matrix of calculations for pancake coil

	Bare Tube	Bare Tube with Sludge	Bare Tube with Roll Transition
Notch TW Depth (%)	0, 100, 60 (ID. and OD.)	0 100	0 100
Coil Position (degrees from notch)	0, 2, 5, 9, 14, 20	0, 2, 5, 9, 14, 20	0
Roll Transition Region (Liftoff Distance: mm)	0.875	0.875	0.875, 1.0, 1.2, 1.4, 1.6, 1.8, 2.0
Sludge Extent	--	4.5, 60, 180^{o}	--
Frequency (kHz)	100/200/300/400	200/400	200/400
Axial Notch Length (mm)	12.7, 30.0	12.7	12.7
Sludge Properties Relative Permeability (no units) Electrical Conductivity [S/mm]	N/A	(10, 100) [1, 100]	N/A

Table 3. Matrix of calculations for T/R probe

	Tube with Notch	Tube with Hole
TW Depth (%)	OD 80/100	OD 80/100
Coil Position (degrees from notch)	0, 2, 5, 9, 14, 20	0, 2, 5, 9, 14, 20
Liftoff Distance (mm)	0.875	0.875
Axial Notch Length (mm)	12.7	--
Hole Diameter (mm)	--	0.90/1.27
Distance between Transmit Coil and Receive Coil (mm)	--	0.75/1.25/1.50/1.75
Frequency (kHz)	200/400	200/400

6. Computation Results and Discussion

The analysis modeled the steam generator tube, the notch, the sludge, and the surrounding air with the ELEKTRA code. To eliminate the effects of mesh coarseness at each point for the field evaluation, the signal from a probe coil over a tube without flaw was subtracted from the signal over the same tube with the flaw being present. The vector potential used over the alloy tubing, notch, and sludge, and the reduced scalar potential was used for the air. The active coil was modeled with a solenoid from the library of available coil shapes. The ELEKTRA solution used the Lorentz gauge solver. Each solution was then repeated with the notch replacing the alloy tubing material. The above computations were carried out at phases 0^{o} and 90^{o}. In all the test cases for pancake coil and the T/R probe, the magnetic flux and the eddy current was displayed, as shown in Figs. 6 and 7 to observe field distributions.

In modeling for the probe response to the presence of the steam generator tubing, a series of probe and tube combinations was set up to compare the effects of key parameters in the EC probe response to notch/sludge geometry (Table 2) and to hole geometry (Table 3). Simulations were performed to model the effect of notch depth and length, hole-diameter, sludge extent, and roll transition at various frequencies. For the test case here, the modeling results were compared between the "flux density integration at phase 0 and 90 degrees" used in the T/R probe (B approach) and "stored-energy/power loss integration" used in the pancake coil (E-P approach). The trends from the predictions of these two approaches are similar, but the amplitude scaling is different.

Figure 8 shows the impedance variations (a) and magnitudes (b) vs. coil lift-off distance for the pancake coil in the roll transition region for frequencies of 200 and 400 kHz. The axial notch is 12.7 mm long and 100% through the tube wall. For this case there is no sludge present outside the tube. Both impedance and amplitude variation are predicted to decrease with increasing lift-off distance at any frequency. Figure 9 displays the amplitudes (a and b) and the impedance diagrams (c and d) of the pancake coil and the T/R probe moving at a constant lift-off distance in the roll transition region for frequencies of 200 and 400 kHz. The tube diameter increases from 19.68 to 20.18 mm over the transition length 6.35 mm. Both the pancake coil probe and the T/R probe predict a stronger signal at middle points and a weaker signal at end points. Simulation results do not show a no significant difference in signal amplitude between 200 and 400 kHz in this specific case.

Figure 10 shows the signal amplitudes of the pancake coil response for axial outer notches of (a) 80%, (b) 60%, and (c) 40% at frequencies of 200 and 400 kHz. Figure 11 shows the signal amplitudes of the T/R probe for axial outer notches of (a) 80%, (b) 60%, and (c) 40% at frequencies of 200 and 400 kHz. For both Fig. 10 (pancake coil) and Fig. 11 (T/R probe) with a

notch length of 12.7 mm and without sludge outside the tube, the signal decreases with decreasing notch TW depth due to skin-depth effect. A stronger signal is observed at the lower frequency (200 kHz) than at the high frequency (400 kHz), again due to skin-depth effect.

For the same test setup shown in Figs. 10 and 11, Fig. 12 displays the impedance diagrams of the pancake coil response and the T/R probe response are shown for axial outer notches (80%, 60%, and 40% TW) at frequencies of 200 and 400 kHz. The length of the impedance curve represents the signal amplitude, and the orientation of the impedance curve indicates the geometrical features of the notch. Results once again indicate that the signal amplitude increases with increasing notch depth and with decreasing frequency.

The signal response was compared between the pancake coil probe (Fig. 13a) and the T/R probe (Fig. 13b) for an axial outer notch of 80% TW and sludge extent of 180^{o} (6.35-mm thick) at frequencies of 200 and 400 kHz. With sludge outside the tube, a strong signal is observed at the lower frequency (e.g., 200 kHz) due to higher depth of penetration. The ratio shown on the figures is defined as the amplitude at 200 kHz to the amplitude at 400 kHz, when the coil is located symmetrically under the notch (coil position 0 degree). Good agreement was observed between a ratio of 1.20 for the E-P approach (pancake coil probe) and 1.18 for the B approach (T/R probe). In Fig. 14, the probe response was also compared between the pancake coil (a and c) and the T/R probe (b and d) for an 80% axial outer notch with and without the sludge at frequencies of 200 and 400 kHz. With high electrical conductivity of the sludge material, more eddy currents flow inside the sludge region. Therefore, in the case of sludge, the signal response is reduced for both the pancake coil probe and the T/R probe due to the lack of currents in the tube to detect the notch.

Figure 15 shows signal amplitudes of the T/R probe for hole diameters of 0.90 mm and 1.27 mm through the wall with T/R separations of 1.25, 1.50, and 1.75 mm at frequencies 200 and 400 kHz. Based on the same test setup for Fig. 15, Fig. 16 displays the impedance diagrams of the T/R probe. The curves from both Figs. 15 and 16 indicate that the signal response increases with decreasing T/R separation and with decreasing frequency for the separation range tested here. Also, the signal response is much stronger for the large hole (diameter of 1.27 mm) than to the small hole (diameter of 0.90 mm).

Figure 17 shows the signal amplitudes of the T/R probe to a hole (diameter of 0.90 mm) with T/R separation of 1.50 mm at frequencies of 200 and 400 kHz. The holes are 100% TW, 80% TW (OD), and 60% TW (ID). In contrast to Figs. 17a and 17b, Fig. 17c is for both T and R coils located on the same side of the hole. Figure 17a shows that the amplitude decreases with increasing frequency for both 100% TW and 80% TW (OD) flaws. Also, the signal amplitude is higher for 100% TW than for 80% TW (OD). In Fig. 17b with 60% TW (ID), there is no significant difference between the amplitudes for 200 and 400 kHz. In Fig. 17c with 60% TW,

the amplitude is much lower for both 200 and 400 kHz, compared with Fig. 17b, because the receiver coil is farther away from the hole.

With the same test setup as Fig. 17, Fig. 18 displays the reactance and resistance profile for (a) 100% TW hole,(b) 80% TW OD hole, and (c) 60% TW ID hole. In Fig. 18, the reactance-resistance variations match well with the amplitude profile in Fig. 17. Also with the same test setup as Figs. 17 and 18, Fig. 19 presents the impedance diagrams of the T/R probe to the hole (0.90-mm diameter) with T/R separation of 1.50 mm and at frequencies of 200 and 400 kHz. Holes are 100% TW, 80% TW (OD), and 60% TW (ID). Based on Figs. 19a and 19b, the impedance curves match well with the amplitude profiles shown in Figs. 17a and 17b. For both 200 and 400 kHz, the impedance curve of the 80% TW (OD) hole is located at the right side of the impedance curve of the 100% TW hole (Figs. 19a and 19b). However, the impedance curves of the 60% TW (ID) hole are located at the left side of the impedance curve of the 100% TW hole (Figs. 19c and 19d). The orientation of the impedance curve is an important clue for judging the radial locations of the notch (inner or outer notch).

Comparing the solutions from the E-P approach (pancake coil) and the B approach (T/R probe) shows that the latter provides similar shapes for the signal response on the impedance diagrams for tests with roll transition, notch depth, and sludge. The scale difference in signal amplitude between the E-P and B-approaches is not a factor to be considered in the modeling validation. The minor inconsistency in signal response diagrams between the two approaches could be caused by a meshing effect. In general, the predictions from the modeling of the T/R probe are qualitatively consistent with the predictions from the modeling of the pancake coil. We conclude from these results that EC NDE modeling is capable of predicting/analyzing the flaws in steam generator tubing and can be used as a tool to analyze the probe response.

These initial test results have led to some fundamental conclusions: (a) as expected, signal strength increases with increasing notch depth, and there is a stronger response to inner notches than to outer notches, (b) signal amplitude increases with increasing sludge extent, (c) signal strength increases with decreasing spacing between the coil and the tube (lift-off) in the roll transition, and (d) signal strength increases with decreasing coil separation for the T/R probe. The results also indicate that for both the pancake coil and the T/R probe, the signal amplitude response from short flaws can be characterized approximately by a Gaussian function. For the coil dimensions used here, an array probe should have no less than about 30 pancake coils to detect all flaws around the circumference. These results show the capability of the 3D FEM-based model in predicting the characteristic response of EC probes to flaws in steam generator tubes. However, further validation calculations must be conducted on real defects, which often exhibit complex geometry that can differ substantially from the manufactured defects in calibration-standard tubes.

7 Summary

A computer model has been developed for predicting the eddy-current coil impedance due to the presence of a notch and a hole in steam generator tubing. Numerical calculations based on steady-state AC theory were completed with a 3-D FEM analysis code for a pancake coil and a T/R probe. Conclusions from the calculations can be summarized as follows:

- The model can predict the EC signal response of notch and hole defects in steam generator tubing.
- The EC signal response increases with increasing notch TW depth, and the signal is stronger with inner notches than with outer notches.
- The probe signal response increases with increasing sludge angles and with decreasing frequency.
- The EC signal increases with decreasing space between the coil and the tube, and with increasing frequency in the roll transitions.
- For the specific pancake coil modeled here, array probe designs should have at least 20 to 30
pancake coils to cover the entire circumference of standard SG tubes..
- The EC signal response is characterized approximately by a Gaussian function for both the pancake coil probe and the T/R probe.

The results from the T/R probe (B-approach) were compared with those from the pancake coil (E-P approach). This comparison showed the consistency between the two approaches. These calculations demonstrate that the 3-D FEM-based solutions can accurately the characteristic response of eddy-current probes to flaws (notch and hole) in steam generator tubes. Additional validation computation must be conducted on more realistic defects in calibration standard tubes. Nevertheless, numerical electromagnetic solutions can be helpful for the interpretation and analysis of eddy-current NDE results.

Acknowledgements

This work was sponsored by the U.S. Department of Energy, Nuclear Energy Plant Optimization (NEPO) program. The authors are grateful for the efforts of Dr. Tom Wei of Reactor Analysis and Engineering, Argonne National Laboratory (ANL). Sincere gratitude and thanks are expressed to Dr. Todd Allen (ANL-Idaho), Dr. James Benson (EPRI), and Dr. B. P. Singh (DOE) for their guidance and support in this project.

References

1. D. S. Kupperman, S. Bakhtiari, and J. Muscara, Status of Argonne Steam Generator Mock-up NDE Round Robin, Proc. 8th Int. Conf. on Nuclear Engineering, Baltimore, MD, April 2-6, 2000, pp. 1-8 (2000).
2. G. Birnbaum and G. Fee, Eddy-Current Characterization of Materials and Structures, American Society for Testing and Materials, Philadelphia, PA, pp. 722 (1981).
3. W. Lord, Eddy Current Methods of Flaw Detection and Their Modeling in *Electromagneto-Mechanical Interactions in Deformable Solids and Structures*, Elsevier Science Publication, Amsterdam, pp. 203-213 (1987).
4. L. R. Turner, *Solving TEAM Problem 8 (Slot in a Plate) on a PC with ELEKTRA*, TEAM Workshop, Okayama University, Okayama, Japan (March 21, 1996).
5. J. R. Pate and C. V. Dodd, Computer Program for Eddy-Current Defect Studies, Oak Ridge National Laboratory Report NUREG/CR-5553 (1990).
6. C. V. Dodd, The Use of Computer-Modeling for Eddy-Current Testing, in *Research Techniques in Nondestructive Testing*, Academic Press, London, Vol. 3, pp. 429-479, Ch. 13 (1977).
7. W. Lord and R. Palanisamy, Development of Theoretical Models for Nondestructive Testing Eddy Current Phenomena, *Eddy-Current Characterization of Materials and Structures*, American Society for Testing and Materials, Philadelphia, PA, pp. 5-21 (1981).
8. C. W. Trowbridge, *An Introduction to Computer Aided Electromagnetic Analysis*, Vector Fields Ltd., Wessex Press, Wantage, Oxon (1990).
9. S. Bakhtiari and D. S. Kupperman, Modeling of Eddy Current Probe Response for Steam Generator Tubes, Nucl. Eng. Design, Vol 194, (1999) 57-71.

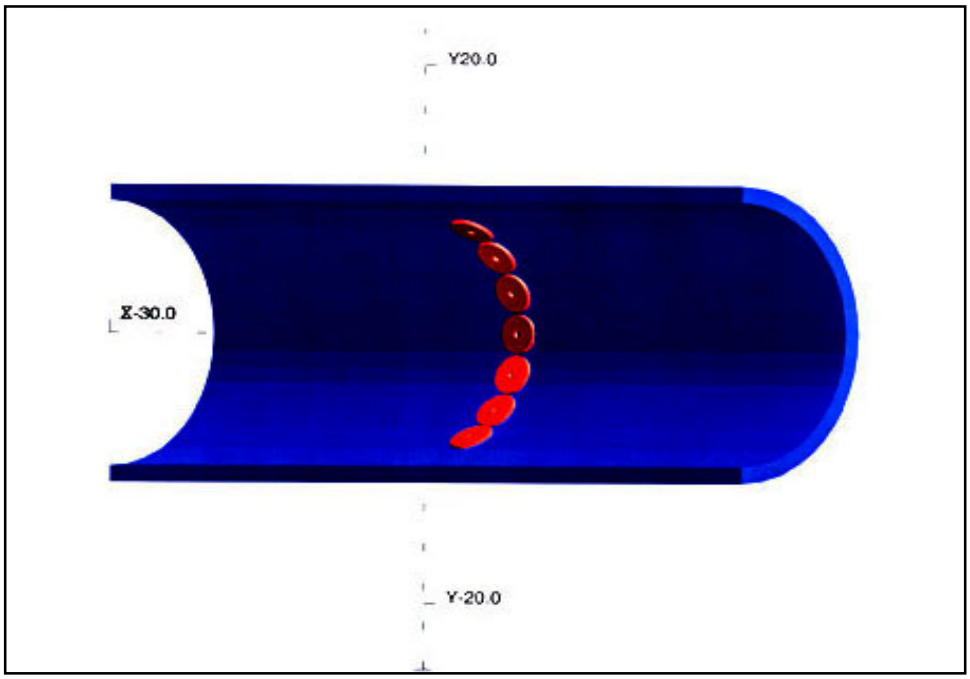

Fig. 1 Pancake coils in array coil configuration

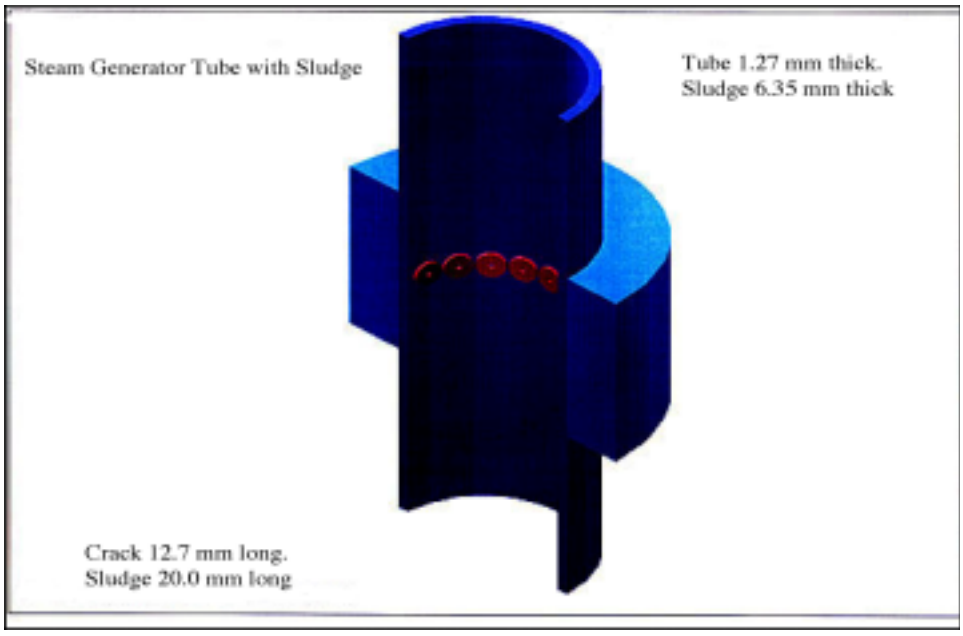

Fig. 2 Configuration of sludge layer and its extent in steam generator tubing

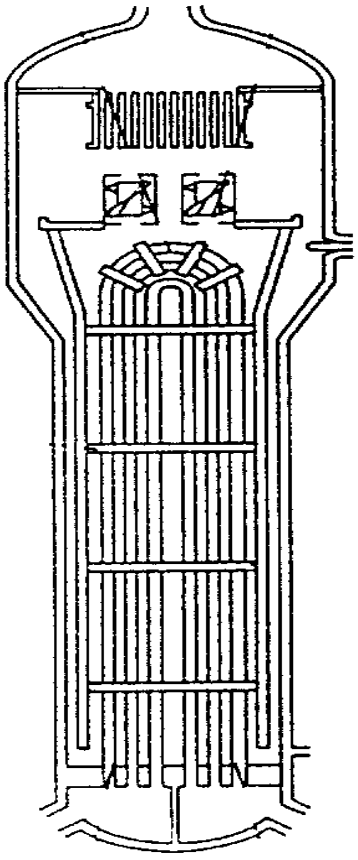

team Generator Tube

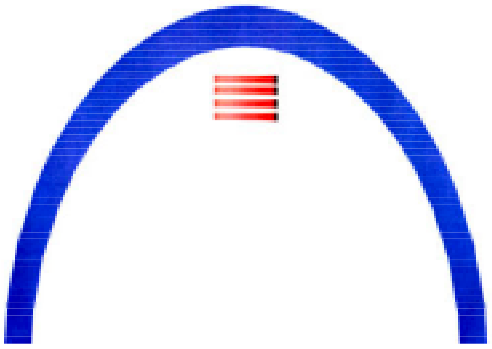

Pancake Coil

d= 0.875, 1.0, 1.2, 1.4, 1.6, 1.8,

Tube ID & OD: 19.66 and 22.22 mm

Fig. 3 Roll transition region and coil lift-off distance in steam generator tubing

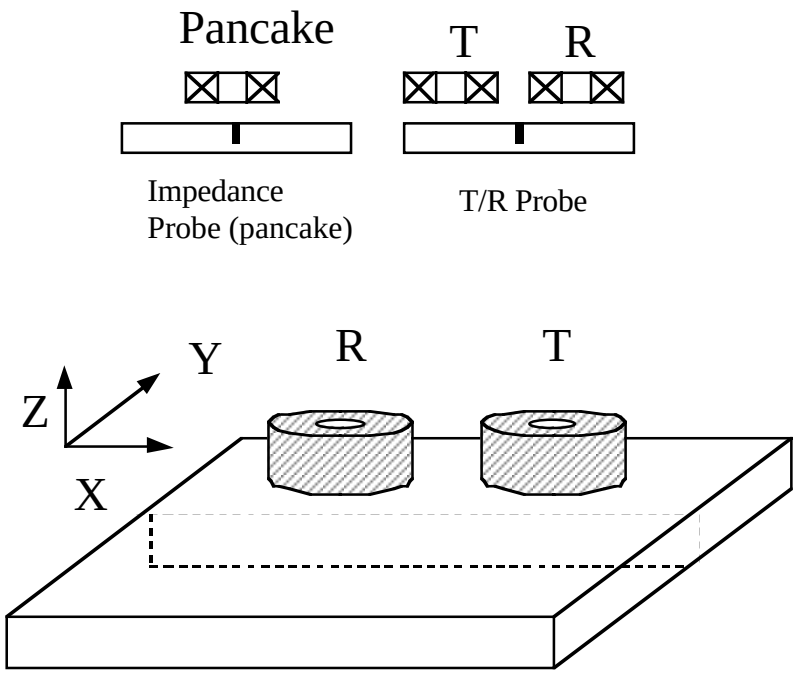

ig. 4. Arrangements of pancake coil and T/R probe in steam generator tubing

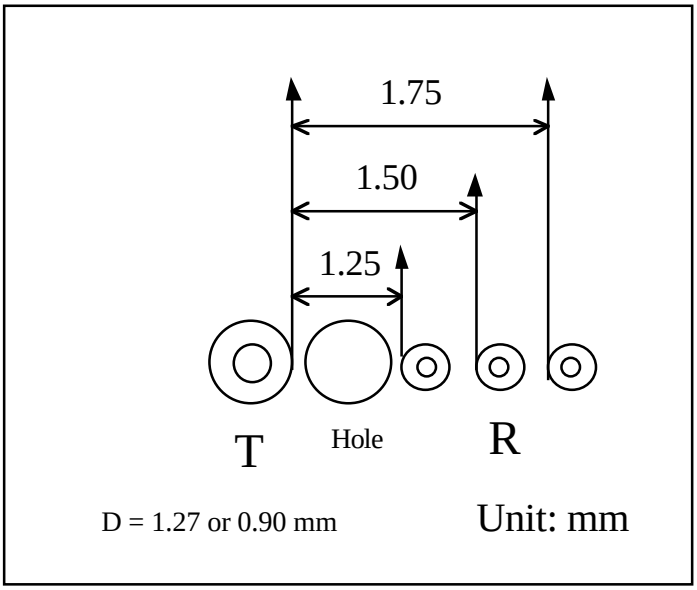

ig. 5. Arrangements of T/R probe for tests with different TW hole diameters and T/R separations in steam generator tubing

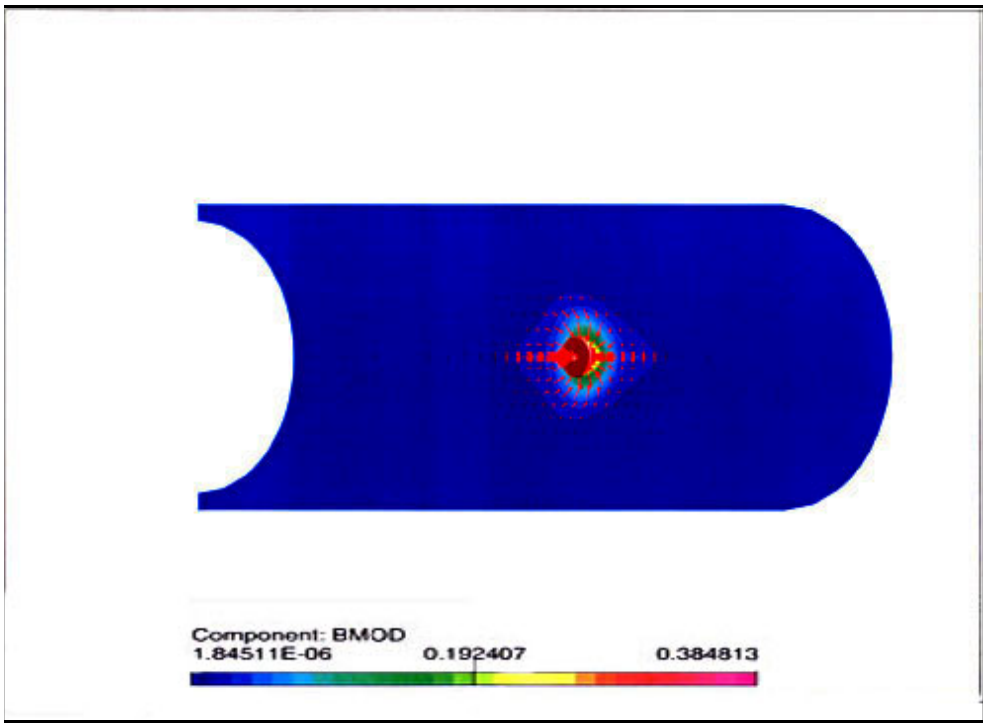

Fig. 6 Magnetic flux density predicted by ELEKTRA in steam generator tubing

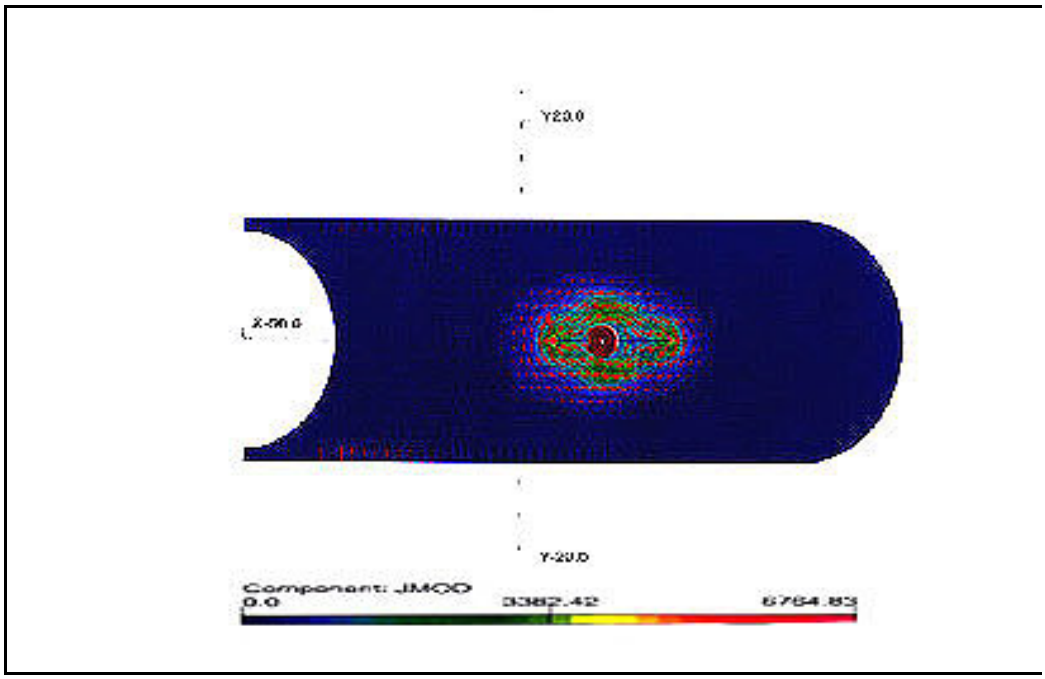

Fig. 7 Current density profile predicted by ELEKTRA in steam generator tubing

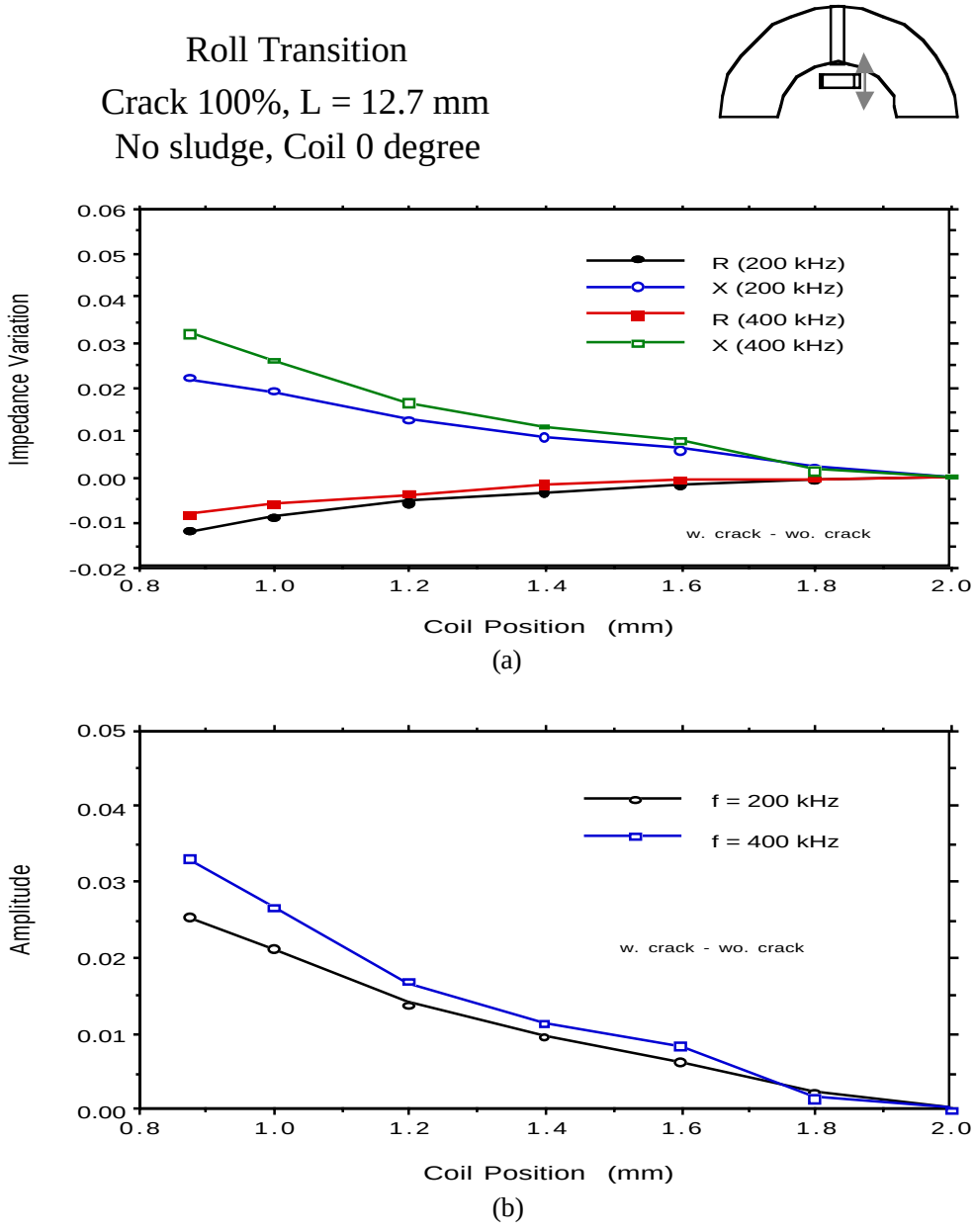

ig. 8. Impedance variations and amplitudes of lift-off effect for pancake coil in the roll transition region at frequencies of 200 and 400 kHz:
(a) Impedance variation vs. coil lift-off distance
(b) Amplitude vs. coil lift-off distance

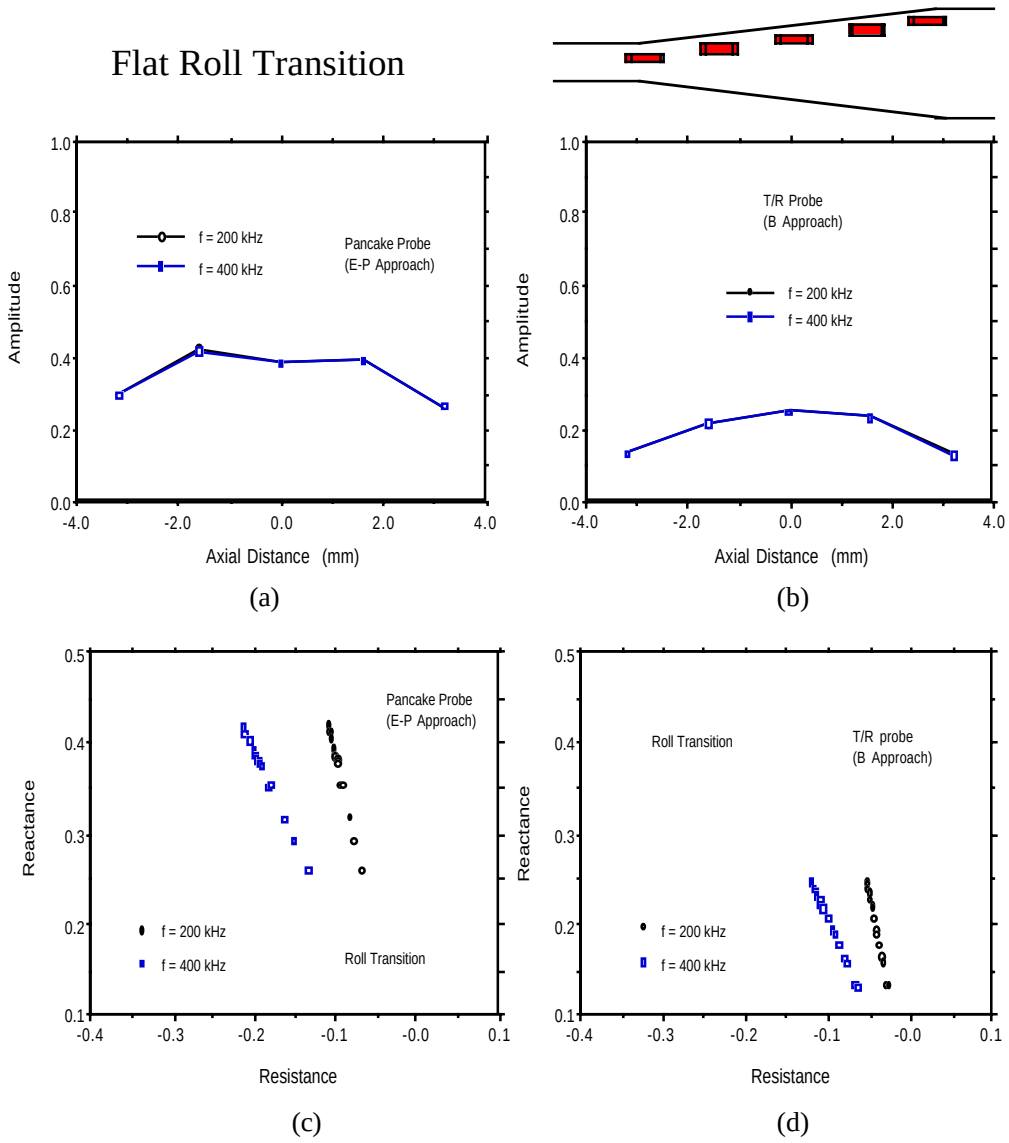

ig. 9. Amplitudes and impedance diagrams of flat-moving pancake coil and T/R probe in the roll transition region at frequencies of 200 and 400 kHz:

(a) Amplitude profile of pancake coil
(b) Amplitude profile of T/R probe
(c) Reactance vs. resistance of pancake coil
(d) Reactance vs. resistance of T/R probe

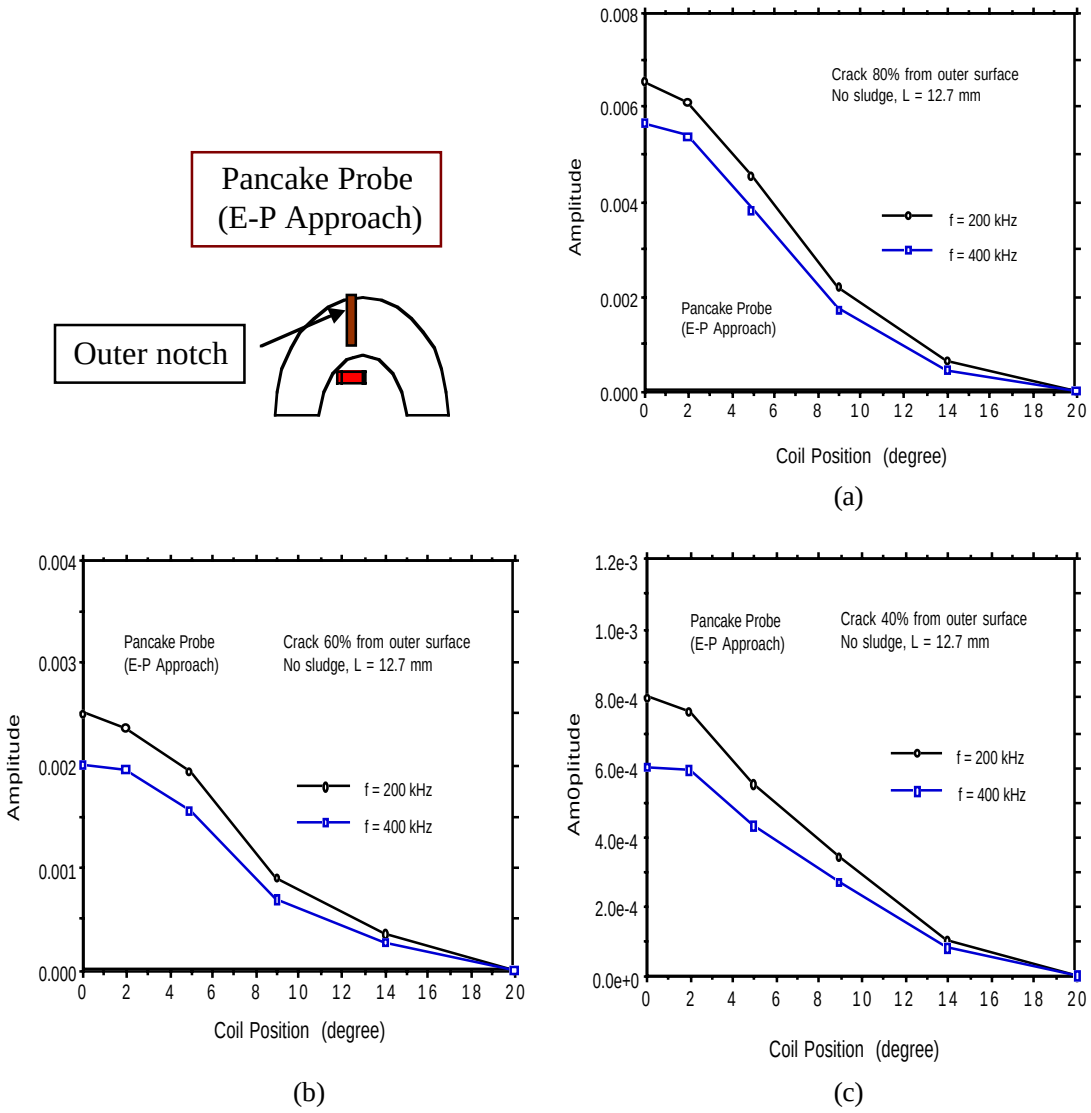

ig. 10. Signal amplitudes of pancake coil for axial outer notches of 80%, 60%, and 40% at frequencies of 200 and 400 kHz

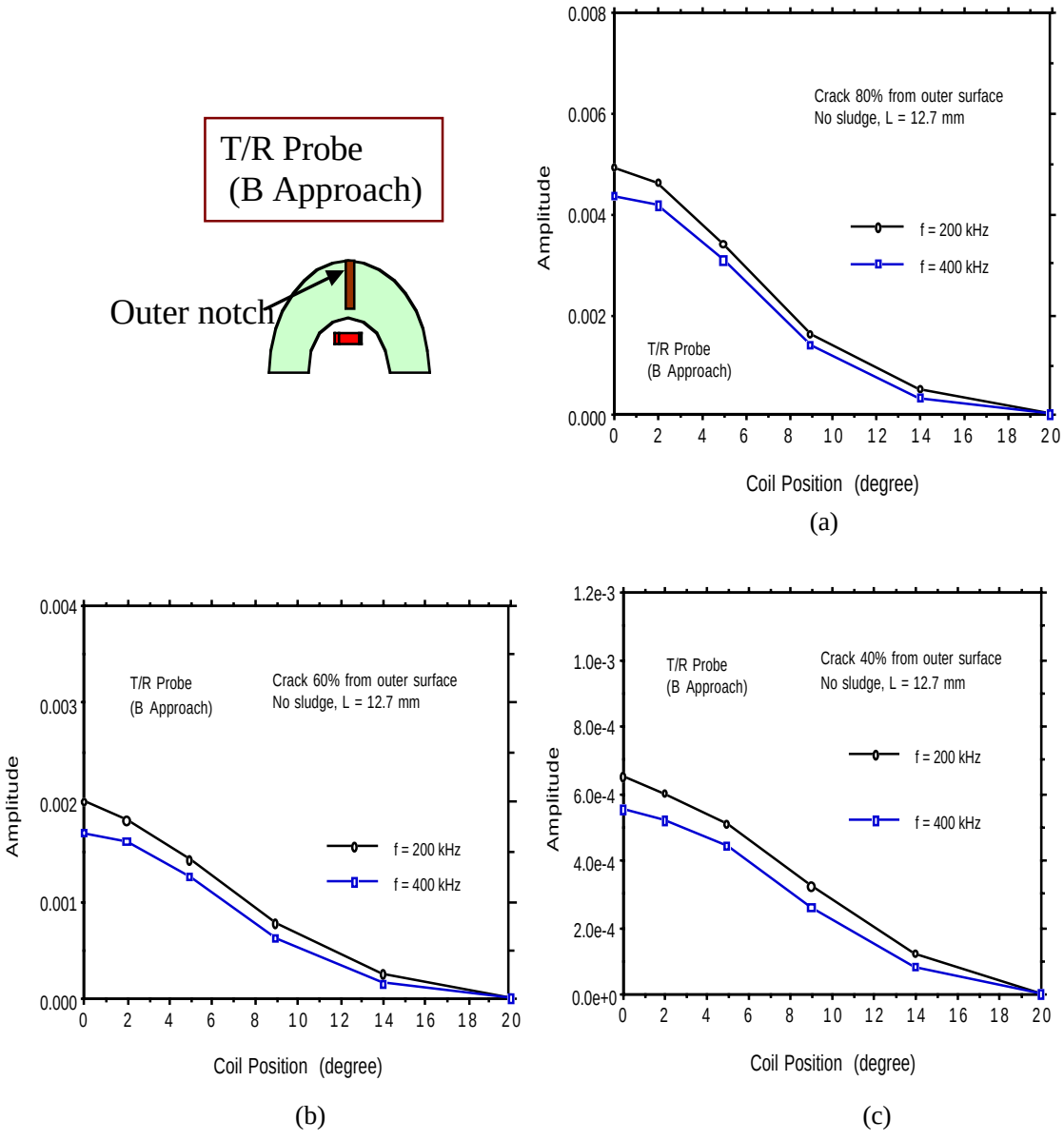

ig. 11. Signal amplitudes of T/R probe for axial outer notches of 80%, 60%, and 40% at frequencies of 200 and 400 kHz

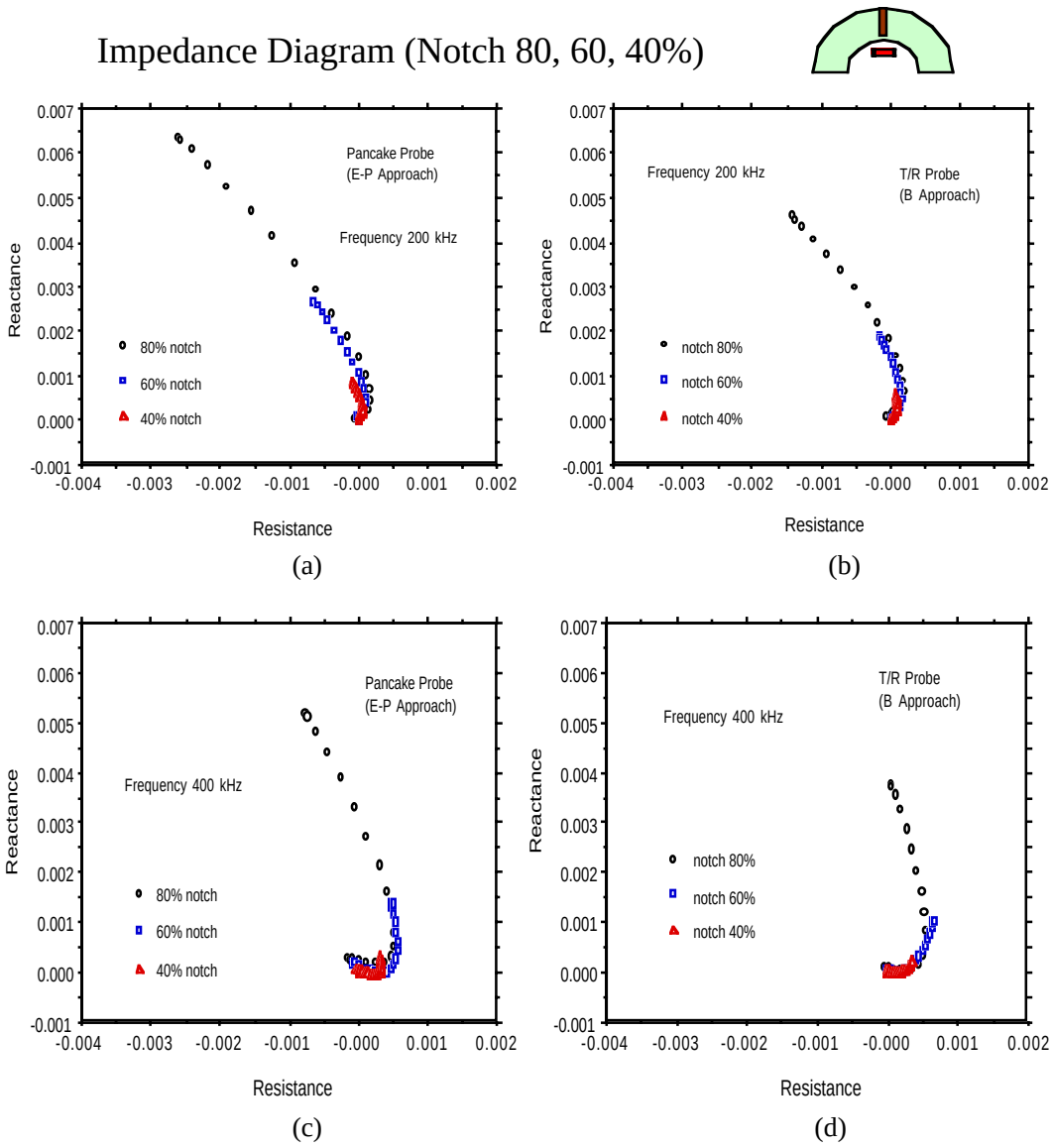

ig. 12. Impedance diagrams of pancake coil and T/R probe for various axial outer notches at frequencies of 200 and 400 kHz:

(a) Pancake probe at 200 kHz

(b) T/R probe at 200 kHz

(c) Pancake probe at 400 kHz

(d) T/R probe at 400 kHz

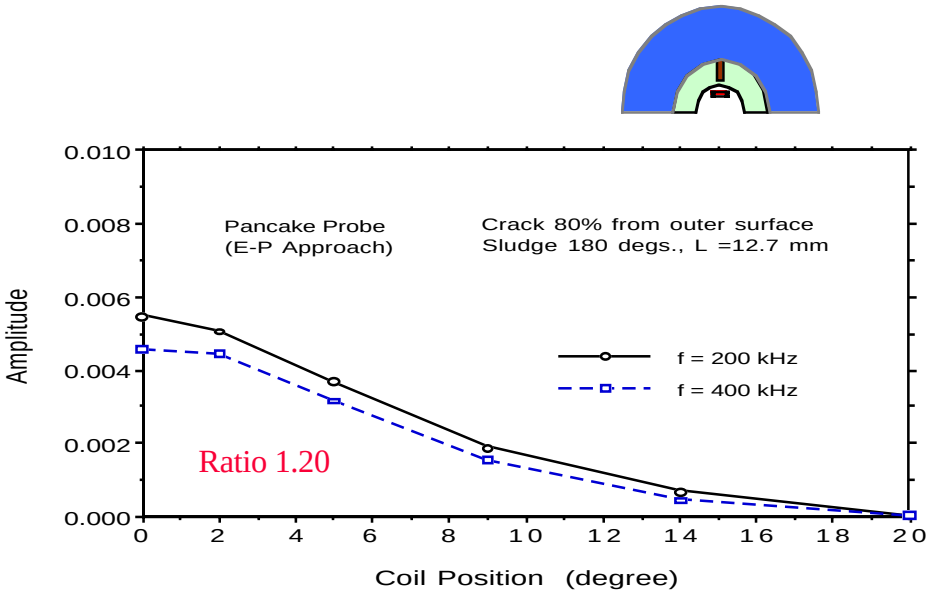

(a)

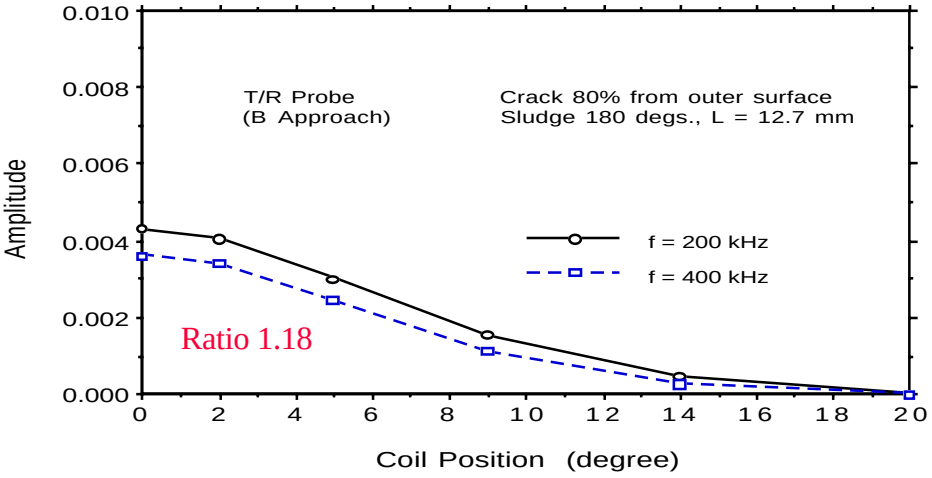

(b)

ig. 13. Signal amplitude between pancake coil and T/R probe for axial outer notch of 80% and sludge extent of 180° at frequencies of 200 and 400 kHz:
(a) Amplitude profile of pancake probe
(b) Amplitude profile of T/R probe

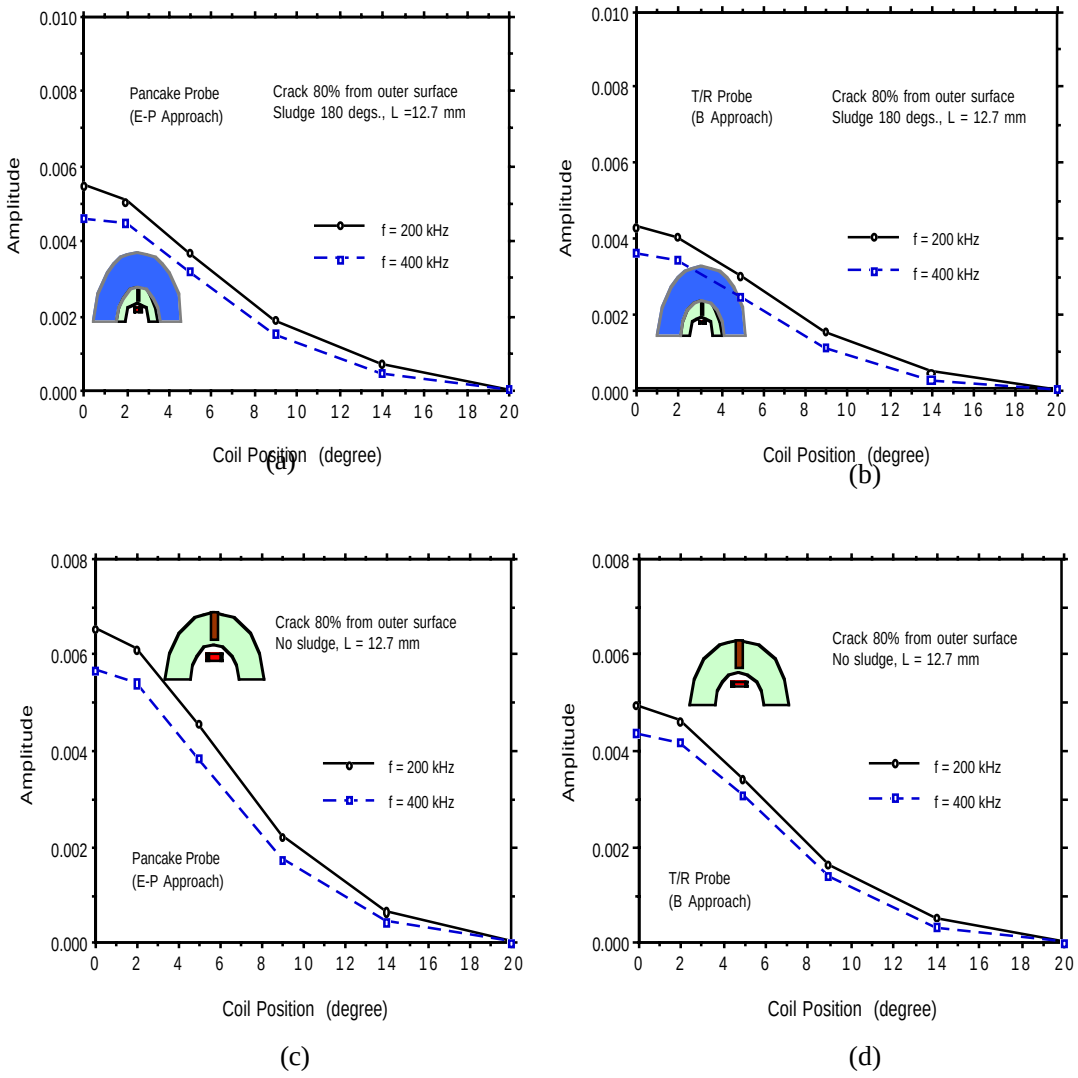

ig. 14. Signal amplitudes between pancake coil and T/R probe for axial outer notch of 80% with and without the sludge at frequencies of 200 and 400 kHz:

(a) Pancake coil response to 80% notch and sludge 180^{o}

(b) T/R probe response to 80% notch and sludge 180^{o}

(c) Pancake coil response to 80% notch without sludge

(d) T/R probe response to 80% notch without sludge

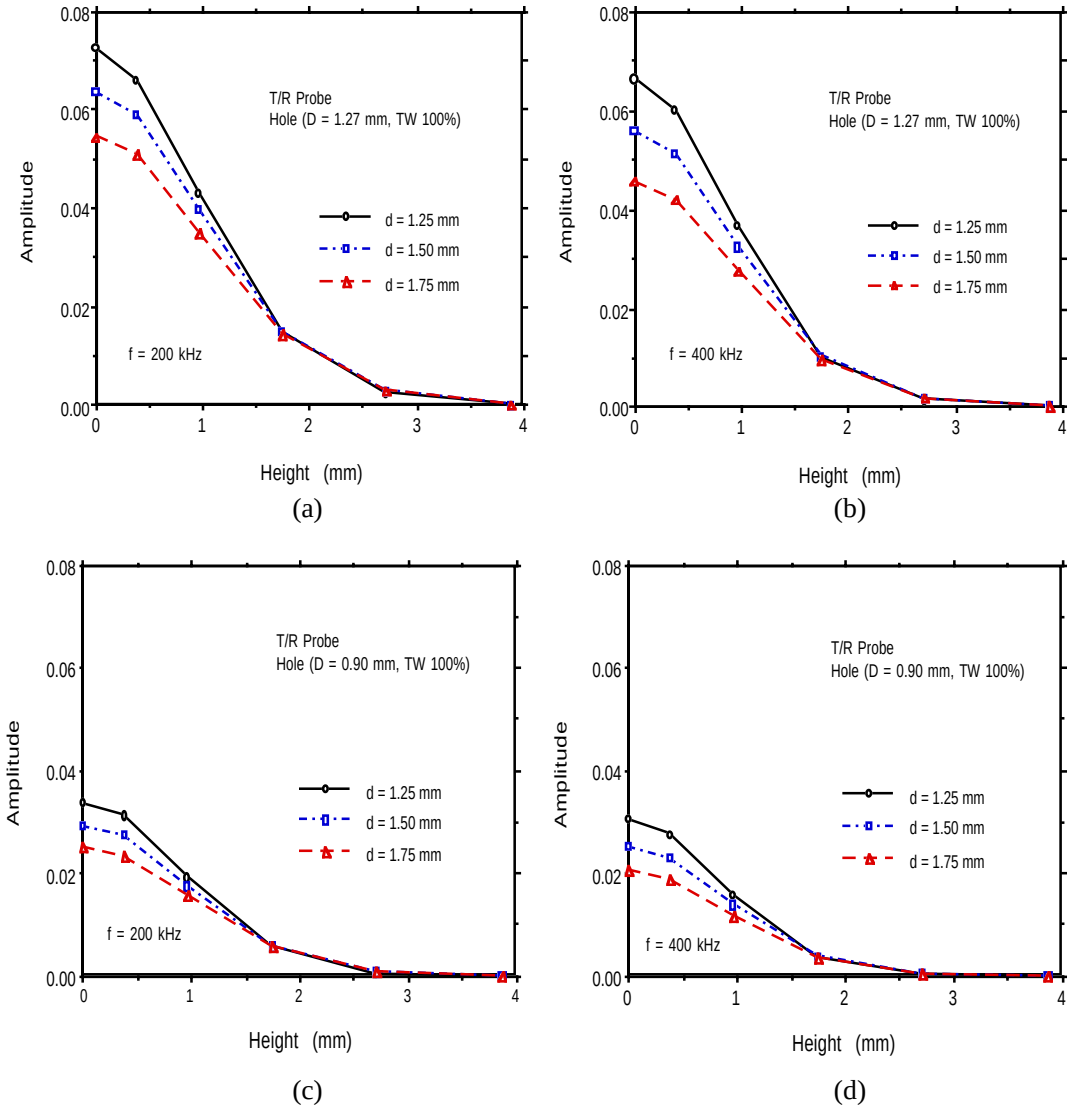

ig. 15. Signal amplitudes of T/R probe for hole diameters of 0.90 mm and 1.27 mm through the wall and the T/R separations of 1.25, 1.50, and 1.75 mm at frequencies of 200 and 400 kHz:

(a) Hole diameter of 1.27 mm and frequency of 200 kHz
(b) Hole diameter of 1.27 mm and frequency of 400 kHz
(c) Hole diameter of 0.90 mm and frequency of 200 kHz
(d) Hole diameter of 0.90 mm and frequency of 400 kHz

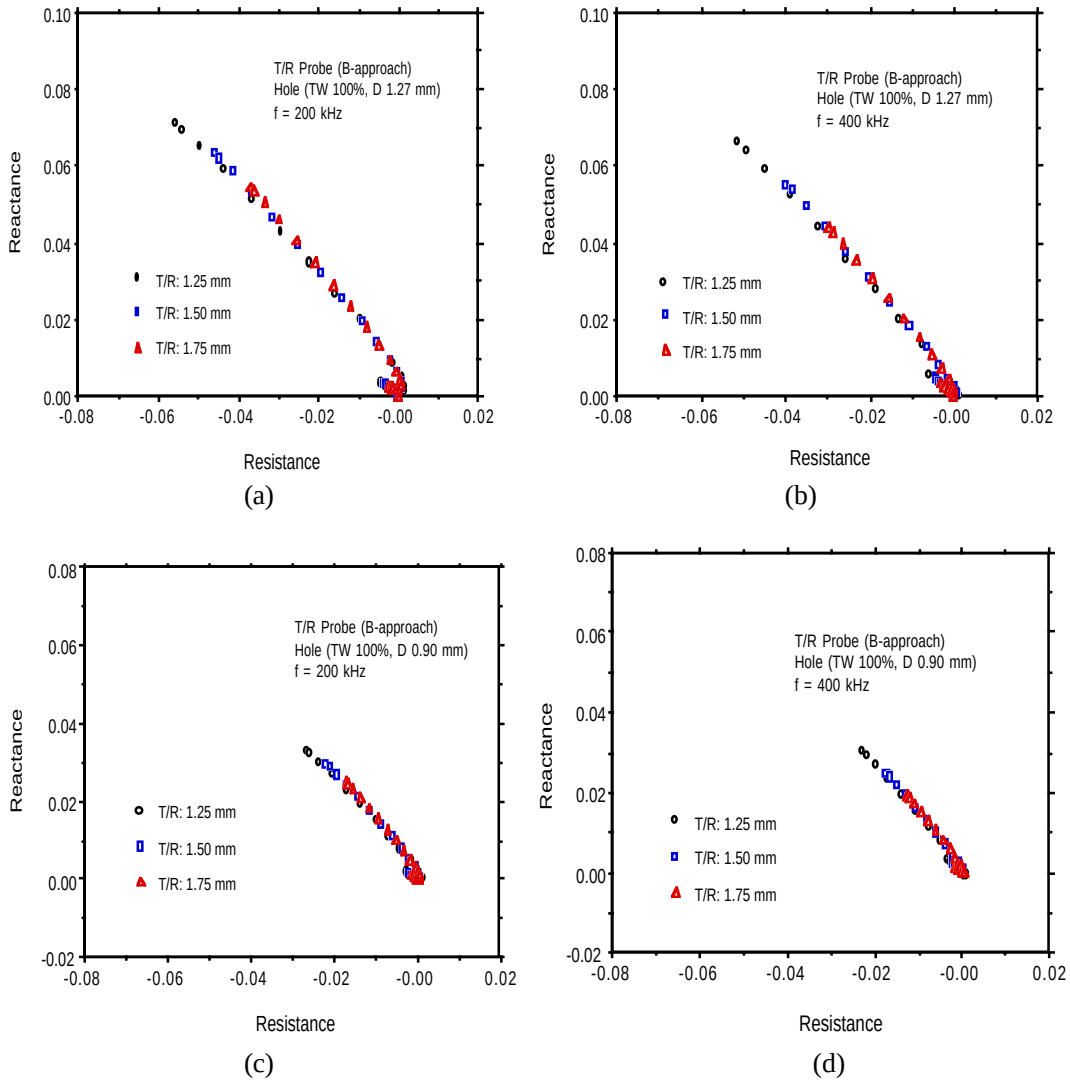

ig. 16. Impedance diagrams of T/R probe for a TW 100% hole with diameters of 1.27 mm and 0.90 mm, frequencies of 200 and 400 kHz, and T/R separations of 1.25, 1.50, and 1.75 mm:

(a) Hole diameter of 1.27 mm and frequency of 200 kHz

(b) Hole diameter of 1.27 mm and frequency of 400 kHz

(c) Hole diameter of 0.90 mm and frequency of 200 kHz

(d) Hole diameter of 0.90 mm and frequency of 400 kHz

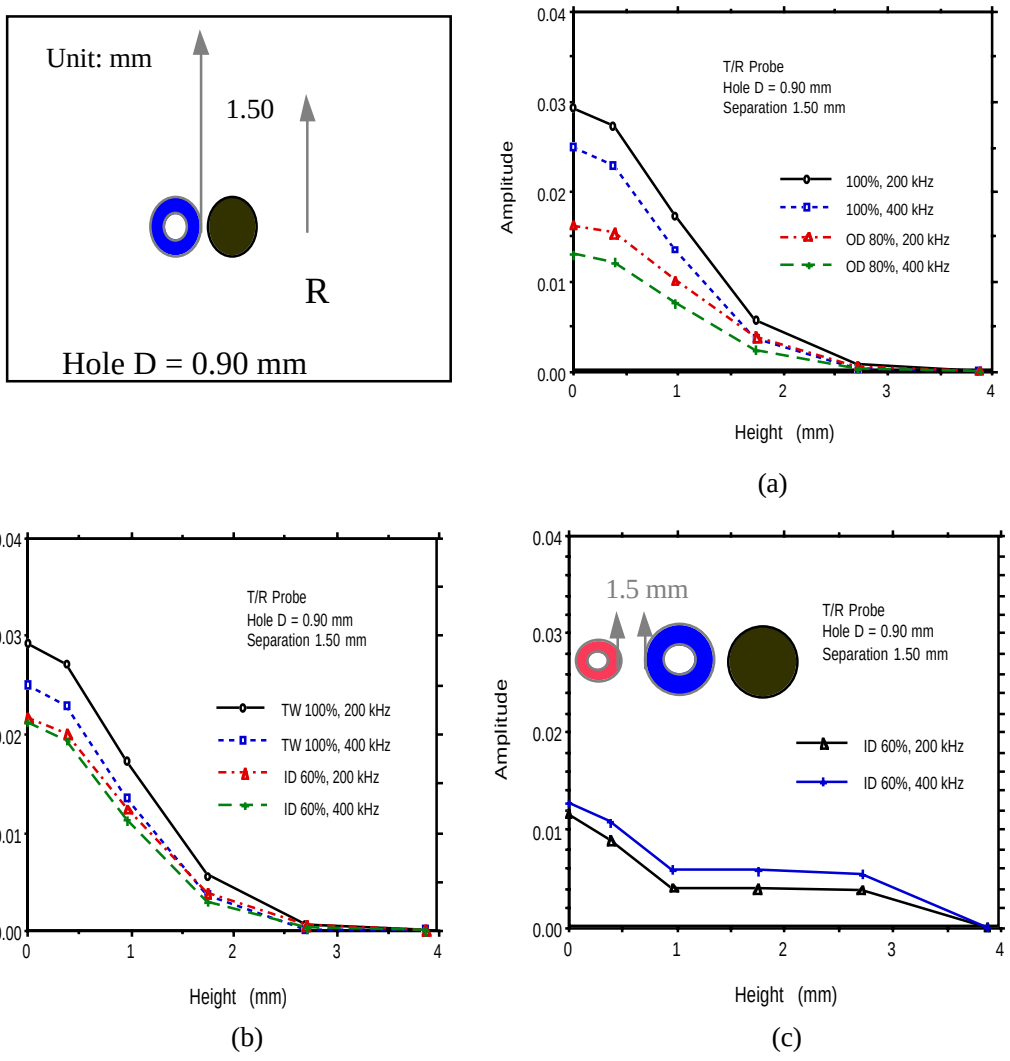

ig. 17. Signal amplitudes of T/R probe for T/R separation of 1.50 mm, frequencies of 200 and 400 kHz, and 0.90-mm diameter holes with TW 100%, TW 80% (OD), and TW 60% (ID):
(a) Holes with TW 100% and TW 80% (OD)
(b) Holes with TW 100% and TW 60% (ID)
(c) Hole with TW 60% and with both T and R coils located at the same side of the hole

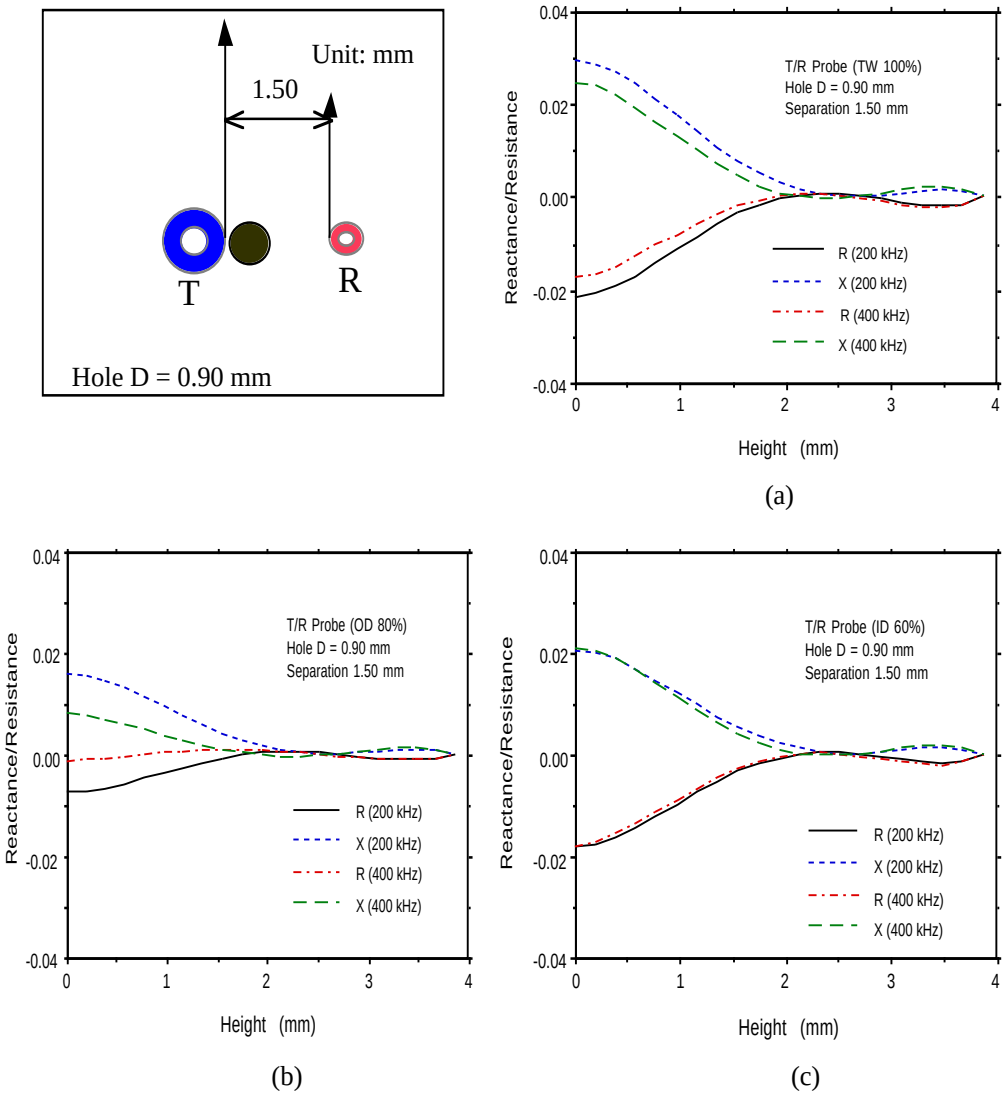

Fig. 18. Reactance and resistance profiles of T/R probe for T/R separation of 1.50 mm, frequencies of 200 and 400 kHz, and 0.90- mm diameter holes with TW 100%, TW 80% (OD), and TW 60% (ID):

(a) Hole with TW 100%
(b) Hole with TW 80% (OD)
(c) Hole with TW 60% (ID)

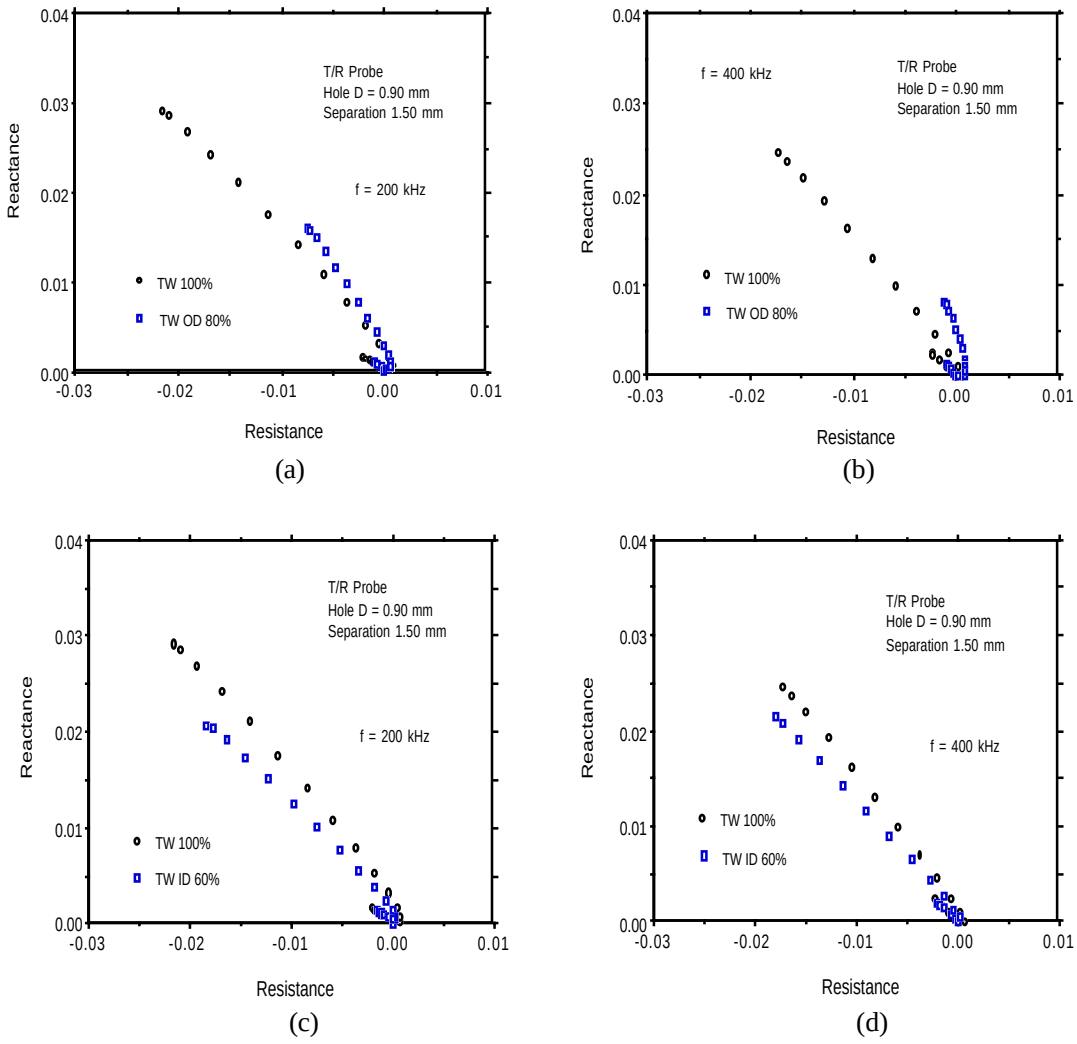

ig. 19. Impedance diagrams of T/R probe for T/R separation of 1.50 mm, frequencies of 200 and 400 kHz, and 0.90-mm diameter holes with TW 100% and TW 80% (OD):

(a) Holes with TW 100% and TW 80% (OD) at 200 kHz

(b) Holes with TW 100% and TW 80% (OD) at 400 kHz

(c) Holes with TW 100% and TW 60% (ID) at 200 kHz

(d) Holes with TW 100% and TW 60% (ID) at 400 kHz

Distribution for ANL-ET/02-27

Internal:

F. C. Chang (5)
S. Bakhtiari (3)
H. Drucker
J. Harmon
A. M. Hassanein (2)
D. S. Kupperman (3)
R. B. Poeppel
A. C. Raptis
R. A. Valentin
N. Zavaljevski
ANL Patent Dept.
ANL Contract File
TIS Files
R. Foote (2)

External:

ANL Libraries
ANL-E
ANL-W
Energy Technology Division Review Committee:
H. K. Birnbaum, University of Illinois, at Urbana-Champaign, IL
I. -W. Chen, University of Pennsylvania
F. P. Ford, Rexford, N.Y.
S. L. Rohde, University of Nebraska-Lincoln
H. S. Rosenbaum, Fremont, CA
S. L. Sass, Cornell University
R. Zoughi, University of Missouri-Rolla